

Supporting Information

Preparation of polymer gold nanoparticle composites with tunable plasmon coupling and their application as SERS substrates

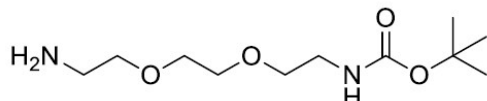
Samir A. Belhout,^a Frederico R. Baptista,^a Stephen J. Devereux,^a Anthony W. Parker,^b Andrew D. Ward^b and Susan J. Quinn^{a*}

^aSchool of Chemistry, University College Dublin, Belfield, Dublin 4, Ireland

^bCentral Laser Facility, Research Complex at Harwell, STFC Rutherford Appleton Laboratory, Harwell Oxford, Didcot OX11 0QX, UK

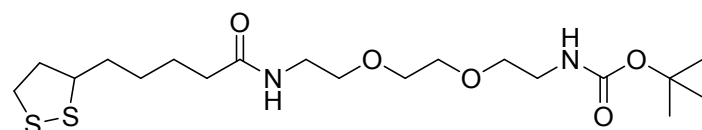
1. Synthesis

Synthesis of *N*-Boc-1,8-diamino-3,6-dioxaoctane¹



(Boc)₂O was added dropwise (2.206 g; 10.1 mmol) in CH₂Cl₂ (50 ml) to a solution of 1,8-diamino-3,6-dioxaoctane (10.7 g; 72.3 mmol) in CH₂Cl₂ (70 ml) at 0 °C. The reaction mixture was stirred for 3 h at room temperature under nitrogen. After that period, the solution was washed with water and brine, the organic layer was dried over MgSO₄. The solvent was evaporated to dryness to afford *N*-Boc-1,8-diamino-3,6-dioxaoctane (1.93 g; 80%) as a colourless oil. ¹H NMR (400 MHz, Chloroform-d): δ = 5.18 (s, 1H), 3.64 – 3.46 (m, 8H), 3.29 (q, *J* = 5.4 Hz, 2H), 2.90 – 2.84 (m, 2H), 2.27 (s, 2H), 1.41 (s, 9H) ppm. ¹³C NMR (101 MHz, Chloroform-d): δ = 156.0, 110.0, 79.1, 77.3, 73.1, 70.2, 41.6, 40.3, 28.4 ppm. HRMS (ESI⁺): *m/z* calc. for C₁₁H₂₄N₂O₄ 248.1736 found 249.1814 (M+H)⁺.

tert-butyl (2-(2-(2-(5-(1,2-dithiolan-3-yl)pentanamido)ethoxy)ethoxy)ethyl)carbamate (1a)²

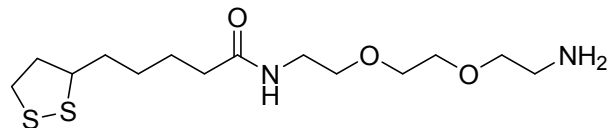


A solution of lipoic acid (0.378 g; 1.8 mmol), Boc-protected diamine (1.02 g; 4.1 mmol), Et₃N (0.75 mL; 5.4 mmol) and EDC (0.702 g; 3.7 mmol) in CH₂Cl₂ (30 mL) was stirred under nitrogen at room temperature for 12 h. After that period, the reaction mixture was evaporated and the residue was purified by column chromatography eluting with CH₂Cl₂:MeOH (93:7) to afford the product as a yellow oil (0.639 g; 80%).

¹H NMR (400 MHz, Chloroform-d) δ 6.04 (bs, 1H), 4.98 (bs, 1H), 3.64 – 3.45 (m, 5H), 3.42 (t, *J* = 5.1 Hz, 4H), 3.29 (q, *J* = 5.6 Hz, 2H), 3.18 – 3.02 (m, 2H), 2.42 (dq, *J* = 12.4, 6.3 Hz, 2H), 2.16 (t, *J* = 7.5 Hz, 2H), 1.91 – 1.83 (m, 2H), 1.74 – 1.57 (m, 4H), 1.41 (s, 11H) ppm. ¹³C NMR (101 MHz, Chloroform-d) δ 172.7, 155.9, 79.3, 77.3, 77.2, 77.0, 76.7, 70.2, 70.1, 69.9, 56.4, 40.3,

40.2, 39.1, 38.4, 36.3, 34.6, 28.9, 28.5, 28.4, 25.3 ppm. **HRMS (ESI⁺)**: *m/z* calc. for C₁₉H₃₆N₂O₅S₂ 436.2066, found 459.1979 (M+Na)⁺.

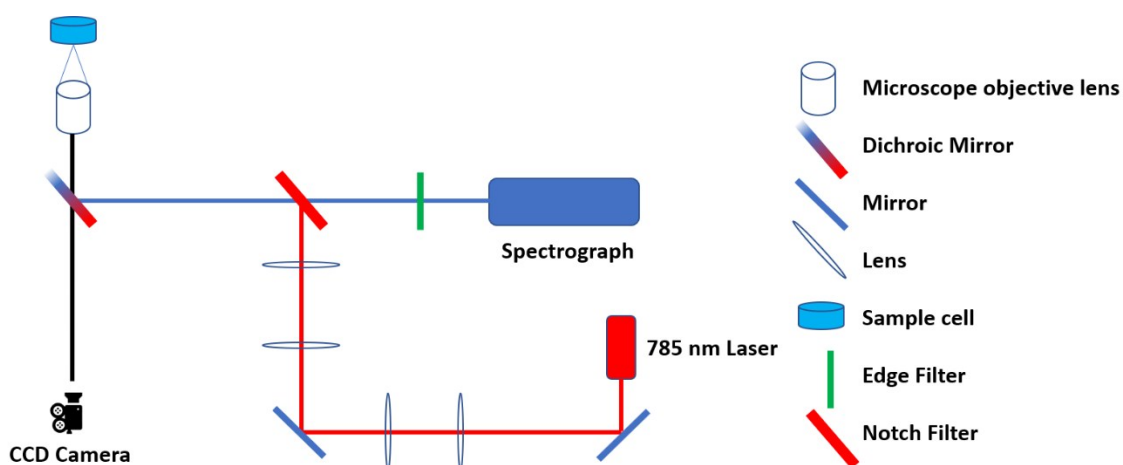
***N*-(2-(2-aminoethoxy)ethoxyethyl)-5-(1,2-dithiolan-3-yl)pentanamide (1)²**



The protected lipoic amine **1a** (0.639; 1.46 mmol) was dissolved in a mixture of TFA:CH₂Cl₂ (4 mL; 1:1) and stirred for 1 h at room temperature. After that period, the mixture was evaporated and purified by column chromatography eluting with CH₂Cl₂:MeOH (75:25) to afford the product as a yellow oil (0.426 g; 83 %). **¹H NMR (400 MHz, Chloroform-d)** δ 8.15 (s, 7H), 6.78 (t, *J* = 5.5 Hz, 2H), 3.76 – 3.34 (m, 29H), 3.21 – 3.03 (m, 10H), 2.63 (td, *J* = 12.1, 10.3, 6.2 Hz, 1H), 2.43 (dq, *J* = 12.5, 6.2 Hz, 2H), 2.19 (t, *J* = 7.5 Hz, 5H), 1.88 (dq, *J* = 13.5, 6.8 Hz, 2H), 1.63 (dtq, *J* = 14.3, 10.5, 7.1, 6.6 Hz, 9H), 1.41 (dq, *J* = 16.2, 8.6, 7.7 Hz, 5H), 1.32 – 1.11 (m, 2H). ppm. **¹³C NMR (101 MHz, Chloroform-d)** δ 174.2, 77.3, 77.2, 77.0, 76.7, 70.2, 70.1, 70.0, 66.7, 56.5, 40.2, 39.5, 39.2, 38.4, 36.3, 36.1, 34.5, 31.5, 31.0, 28.8, 25.4 ppm. **HRMS (ESI⁺)**: *m/z* calc. for C₁₄H₂₈N₂O₃S₂ 336.1541, found 337.1612 (M+H)⁺.

Table S1 Concentrations of 200 nm PSLA and 5.3 μm PSLA used for composite formation

	200 nm PSLA	5.3 μm PSLA
13 nm AuNPs	1.0 × 10 ⁻² % (w/v) PS	0.15 % (w/v) PS
17 nm AuNPs	8.4 × 10 ⁻³ % (w/v) PS	0.16 % (w/v) PS
22 nm AuNPs	7.7 × 10 ⁻³ % (w/v) PS	0.14 % (w/v) PS
26 nm AuNPs	6.5 × 10 ⁻³ % (w/v) PS	-
30 nm AuNPs	6.6 × 10 ⁻³ % (w/v) PS	0.12 % (w/v) PS



Scheme S1. Schematic representation of set-up for single particle Raman measurements

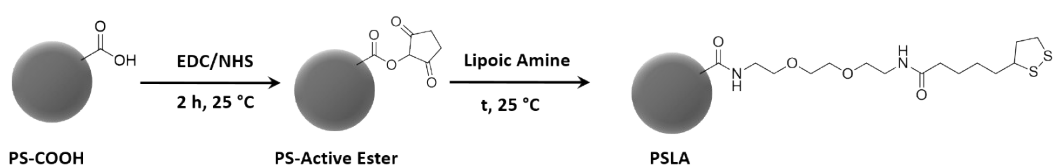


Figure S1. Reaction scheme showing the formation of lipoic amine functionalised PS beads (PSLA)

2. Materials Characterisation

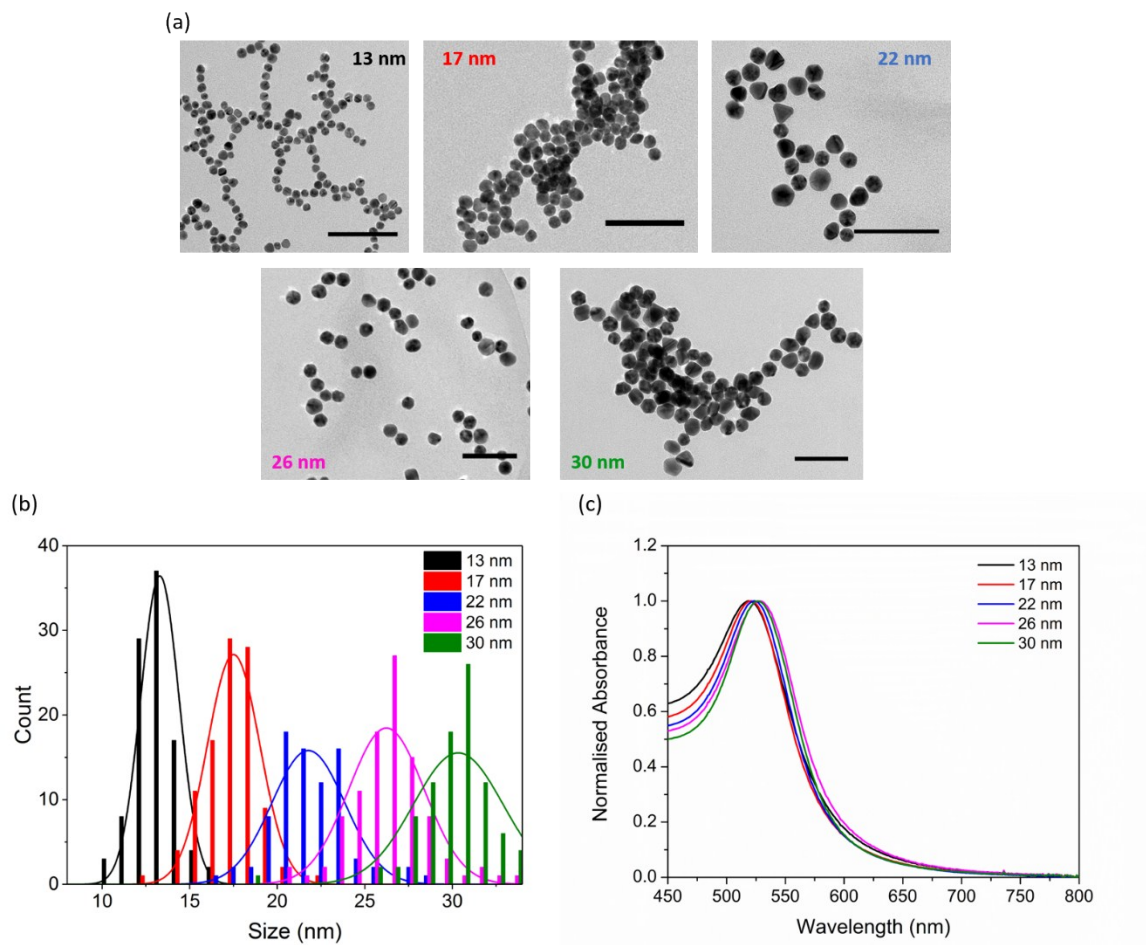


Figure S2. (a) TEM images (b) histogram of Au core size by TEM and (c) UV-visible spectra of AuNPs synthesised via the Bastús *et al.* preparation. Scale bar in each image represents 100 nm.³

Table S2. Summary of properties of AuNPs synthesised via the Bastús preparation.

Family	13 nm	17 nm	22 nm	26 nm	30 nm
Size by TEM	13 ± 1 nm	17 ± 2 nm	22 ± 2 nm	26 ± 2 nm	30 ± 3 nm
λ_{max}	517 nm	520 nm	522 nm	525 nm	527 nm
Au conc.	126 ± 11 mg/L	170 ± 21 mg/L	201 ± 14 mg/L	215 ± 22 mg/L	219 ± 18 mg/L
ϵ ($M^{-1} cm^{-1}$)	$(2.46 \pm 0.21) \times 10^8$	$(6.01 \pm 0.74) \times 10^8$	$(1.41 \pm 0.10) \times 10^9$	$(2.76 \pm 0.28) \times 10^9$	$(3.96 \pm 0.33) \times 10^9$

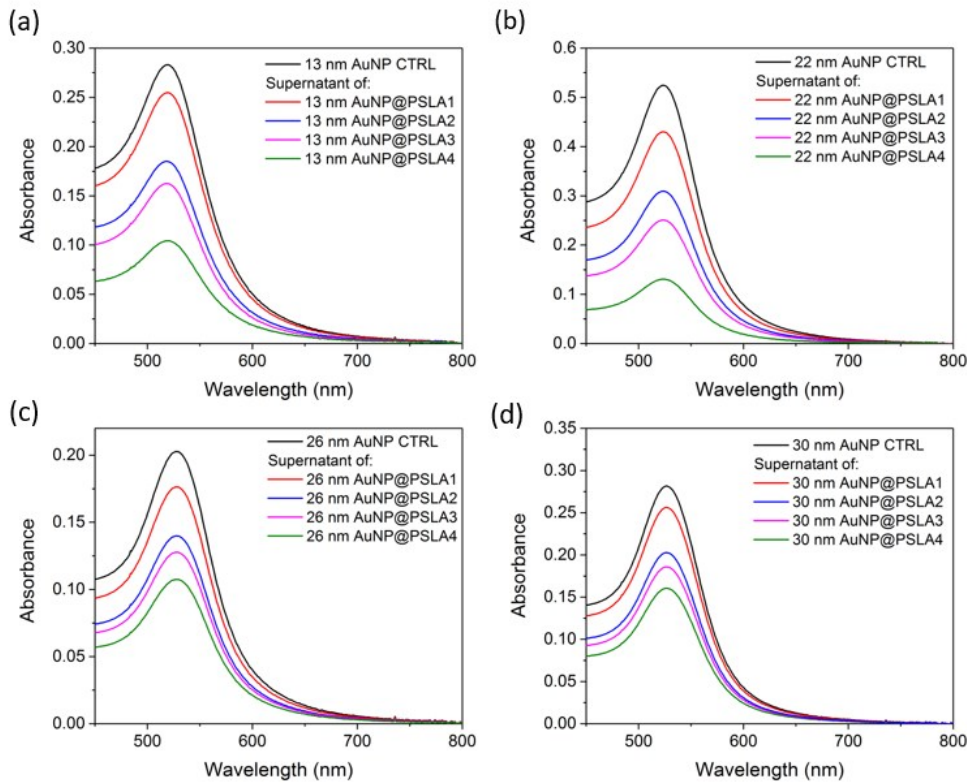


Figure S3. UV-visible of spectra of control and supernatant of (a) 13 nm, (b) 22 nm, (c) 26 nm and (d) 30 nm AuNPs after composite formation with PSLA1-4.

Table S3. Summary of loadings, in % PS surface area covered, for the different AuNP sizes and PSLA families.

	13 nm AuNP	17 nm AuNP	22 nm AuNP	26 nm AuNP	30 nm AuNP
PSLA1	3.0 %	4.2 %	5.5 %	4.1 %	3.7 %
PSLA2	9.6 %	11.3 %	12.9 %	10.5 %	9.1 %
PSLA3	11.3 %	13.4 %	16.8 %	12.9 %	11.1 %
PSLA4	16.8 %	20.4 %	23.3 %	16.2 %	15.2 %

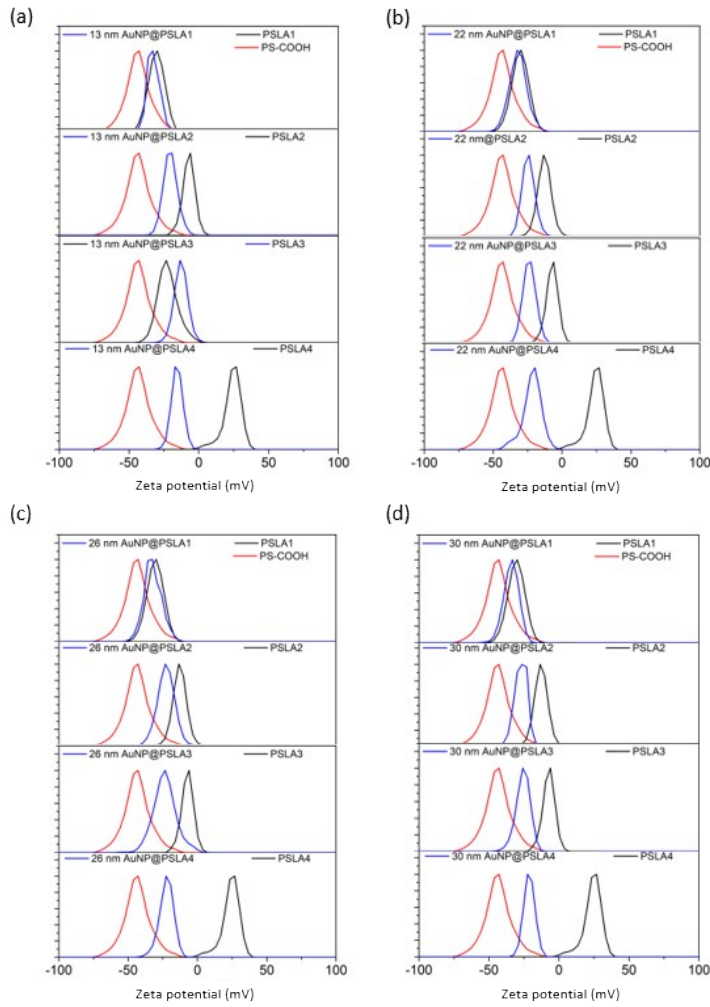


Figure S4. ζ -potential measurements of (a) 13 nm, (b) 22 nm, (c) 26 nm and (d) 30 nm AuNPs immobilised on PSLA1-4 taken in Millipore H₂O at pH 7.

Table S4. Summary of ζ -potential change upon composite formation for all families.

	13 nm AuNP	17 nm AuNP	22 nm AuNP	26 nm AuNP	30 nm AuNP
PSLA1	-2 mV	-3 mV	-2 mV	-3 mV	-4 mV
PSLA2	-9 mV	-13 mV	-9 mV	-13 mV	-15 mV
PSLA3	-16 mV	-21 mV	-17 mV	-21 mV	-21 mV
PSLA4	-42 mV	-46 mV	-51 mV	-53 mV	-50 mV

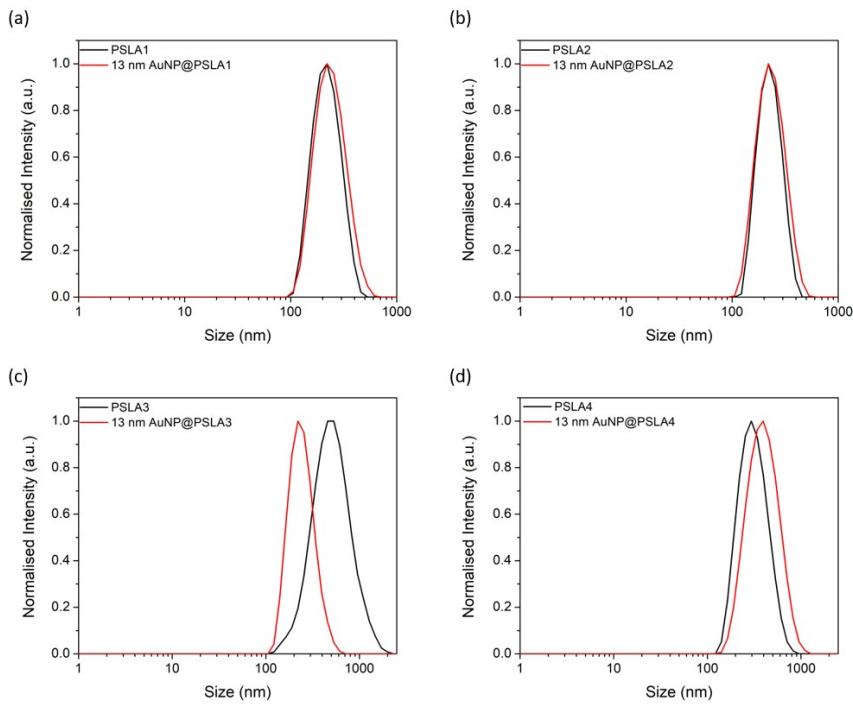


Figure S5. DLS measurements of 13 nm AuNP@ (a) PSLA1, (b) PSLA2, (c) PSLA3 and (d) PSLA4 composite materials taken in ddH₂O at pH 7.

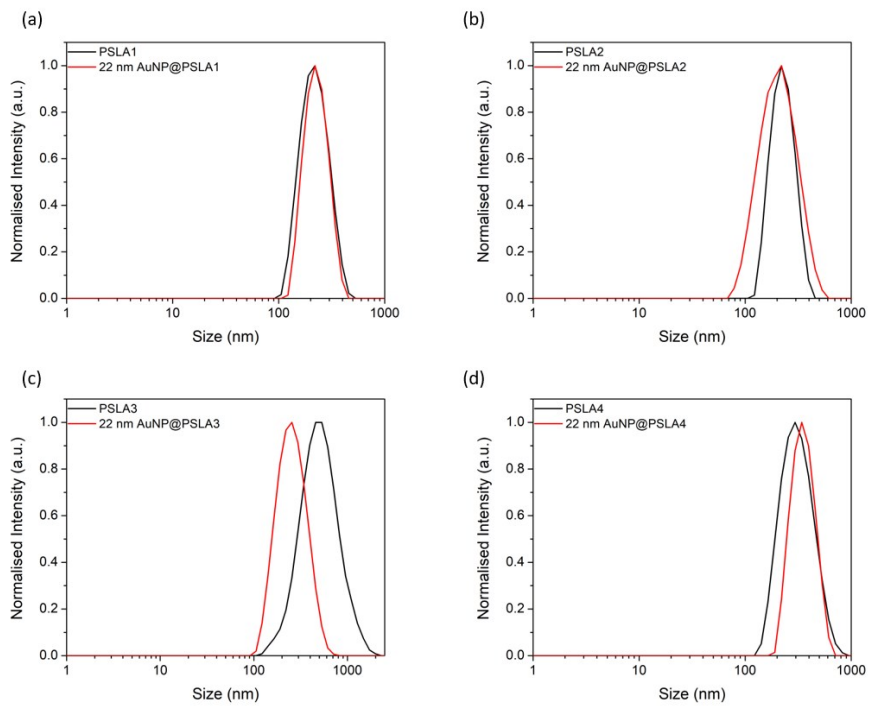


Figure S6. DLS measurements of 22 nm AuNP@ (a) PSLA1, (b) PSLA2, (c) PSLA3 and (d) PSLA4 composite materials taken in ddH₂O at pH 7.

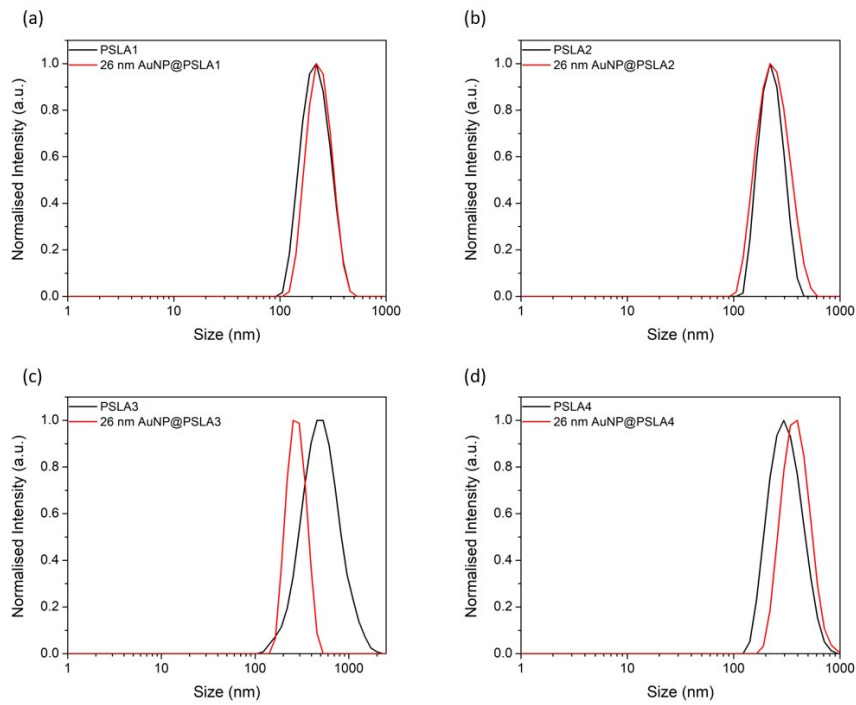


Figure S7. DLS measurements of 26 nm AuNP@ (a) PSLA1, (b) PSLA2, (c) PSLA3 and (d) PSLA4 composite materials taken in ddH₂O at pH 7.

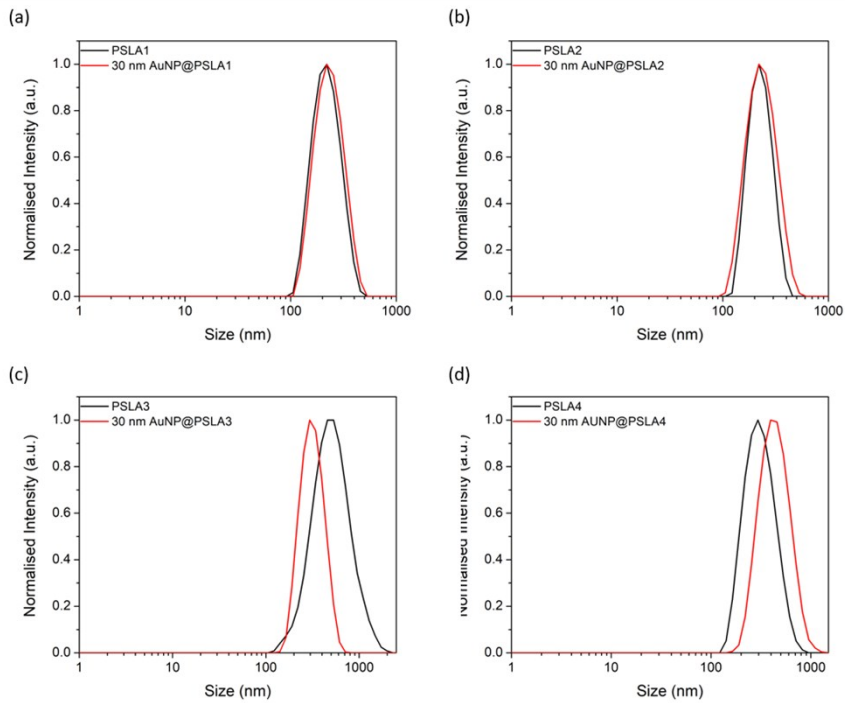


Figure S8. DLS measurements of 30 nm AuNP@ (a) PSLA1, (b) PSLA2, (c) PSLA3 and (d) PSLA4 composite materials taken in ddH₂O at pH 7.

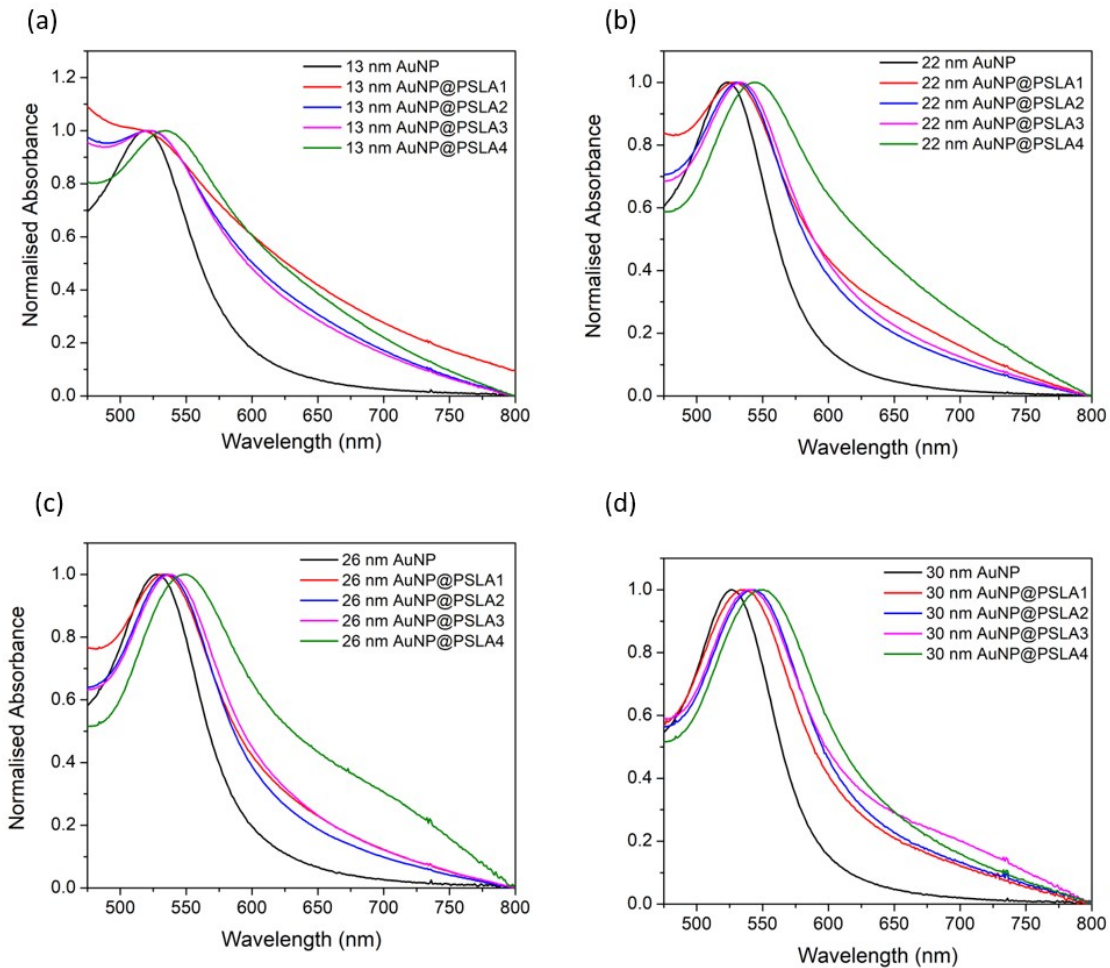


Figure S9. UV-visible spectra of composite materials formed using (a) 13 nm, (b) 22 nm, (c) 26 nm and (d) 30 nm AuNPs taken in Millipore H₂O

Table S5. Summary of surface plasmon peak positions (λ_{SPR}) of different composite families

	free AuNP	PSLA1	PSLA2	PSLA3	PSLA4
13 nm AuNP	517 nm	518 nm	521 nm	523 nm	532 nm
17 nm AuNP	520 nm	524 nm	527 nm	530 nm	538 nm
22 nm AuNP	522 nm	527 nm	531 nm	533 nm	544 nm
26 nm AuNP	525 nm	531 nm	535 nm	538 nm	549 nm
30 nm AuNP	527 nm	533 nm	540 nm	543 nm	552 nm

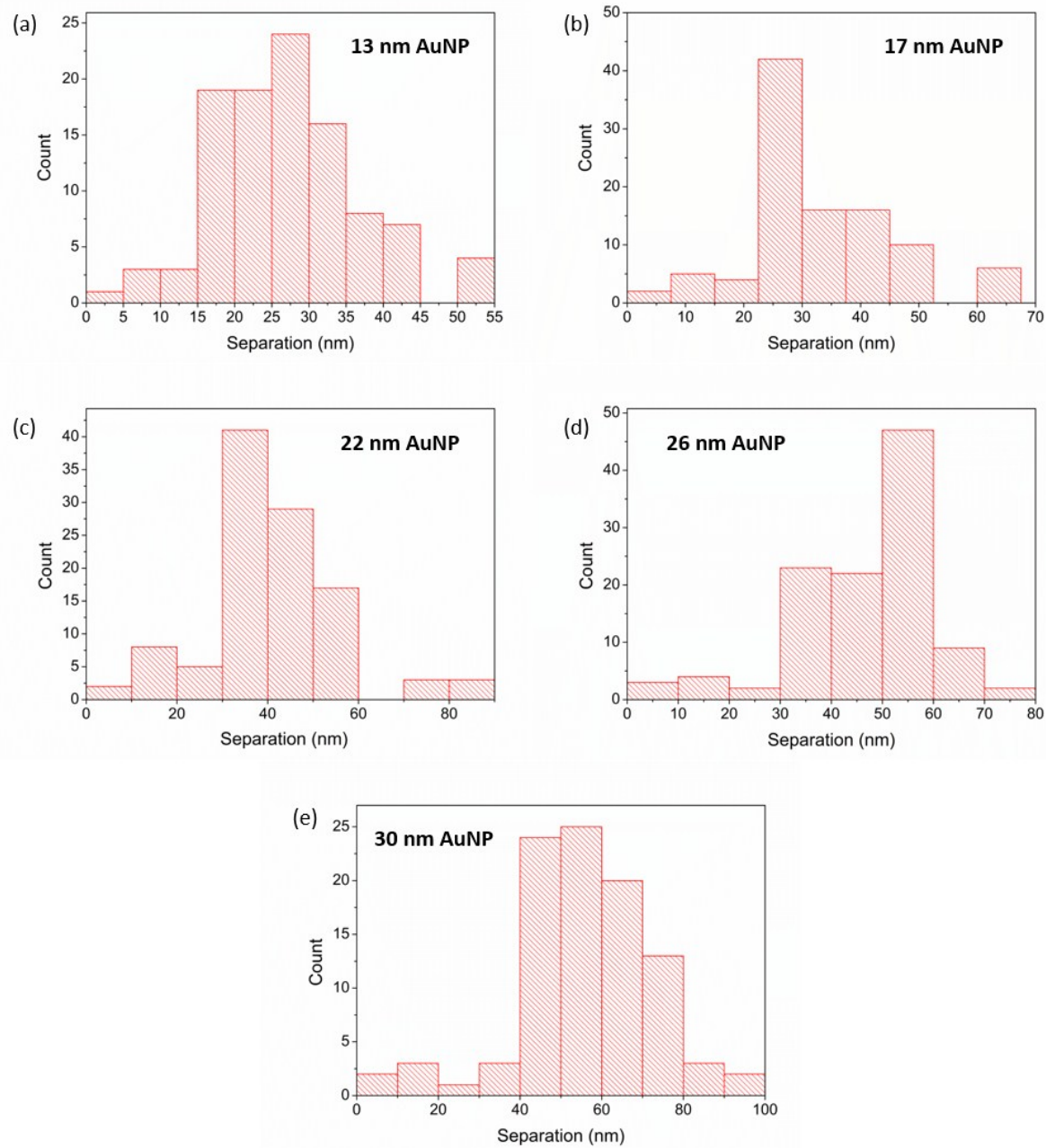


Figure S10. Histogram of the interparticle separation obtained from SEM images for (a) 13 nm AuNPs, (b) 17 nm AuNPs, (c) 22 nm AuNPs, (d) 26 nm AuNPs and (e) 30 nm AuNPs immobilised on **PSLA1** beads.

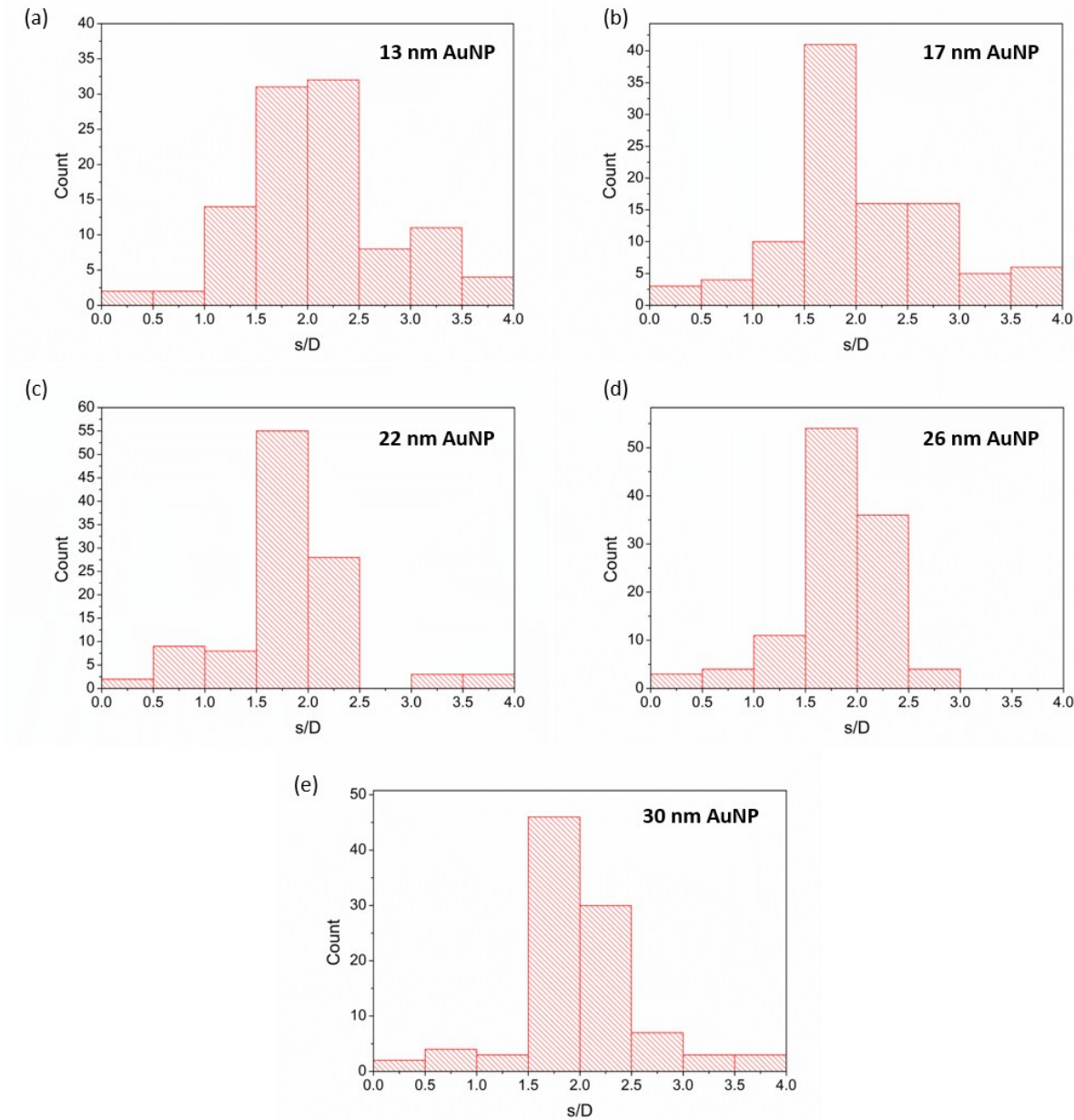


Figure S11. Histogram of relative interparticle separation ($s = \text{interparticle distance}$, $D = \text{diameter}$) measured for (a) 13 nm AuNPs, (b) 17 nm AuNPs, (c) 22 nm AuNPs, (d) 26 nm AuNPs and (e) 30 nm AuNPs immobilised on **PSLA1** beads.

Table S6. Summary of interparticle distance for various composites as measured by SEM.

	13 nm AuNPs	17 nm AuNPs	22 nm AuNPs	26 nm AuNPs	30 nm AuNPs
PSLA1	28.7 ± 18.5 nm	34.3 ± 12.3 nm	41.4 ± 12.9 nm	42.8 ± 15 nm	47.4 ± 16.6 nm
PSLA1*	16.3 ± 3.7 nm	18.7 ± 2.4 nm	25.8 ± 9.5 nm	29.2 ± 3.9 nm	34.8 ± 4.2 nm
PSLA2	6.6 ± 2.0 nm	9.6 ± 2.1 nm	12.6 ± 2.3 nm	13.6 ± 2.7 nm	15.8 ± 4.6 nm
PSLA3	5.1 ± 1.5 nm	7.0 ± 1.3 nm	8.4 ± 1.5 nm	10.3 ± 1.6 nm	10.5 ± 2.9 nm
PSLA4	3.3 ± 0.7 nm	3.8 ± 0.7 nm	4.0 ± 0.5 nm	5.0 ± 1.1 nm	5.4 ± 1.2 nm

* AuNPs falling outside $1.5D$ were normalised to $1.5D$.

Table S7. Summary of relative interparticle separation as a function of AuNP size (s/D) for each AuNP@PSLA composite family.

	PSLA1	PSLA2	PSLA3	PSLA4
13 nm AuNP	1.25 ± 0.28	0.514 ± 0.157	0.413 ± 0.118	0.257 ± 0.056
17 nm AuNP	1.10 ± 0.21	0.566 ± 0.124	0.413 ± 0.074	0.222 ± 0.0386
22 nm AuNP	1.13 ± 0.19	0.574 ± 0.106	0.384 ± 0.067	0.183 ± 0.024
26 nm AuNP	1.12 ± 0.15	0.524 ± 0.102	0.395 ± 0.0617	0.192 ± 0.042
30 nm AuNP	1.16 ± 0.14	0.527 ± 0.152	0.348 ± 0.096	0.181 ± 0.041

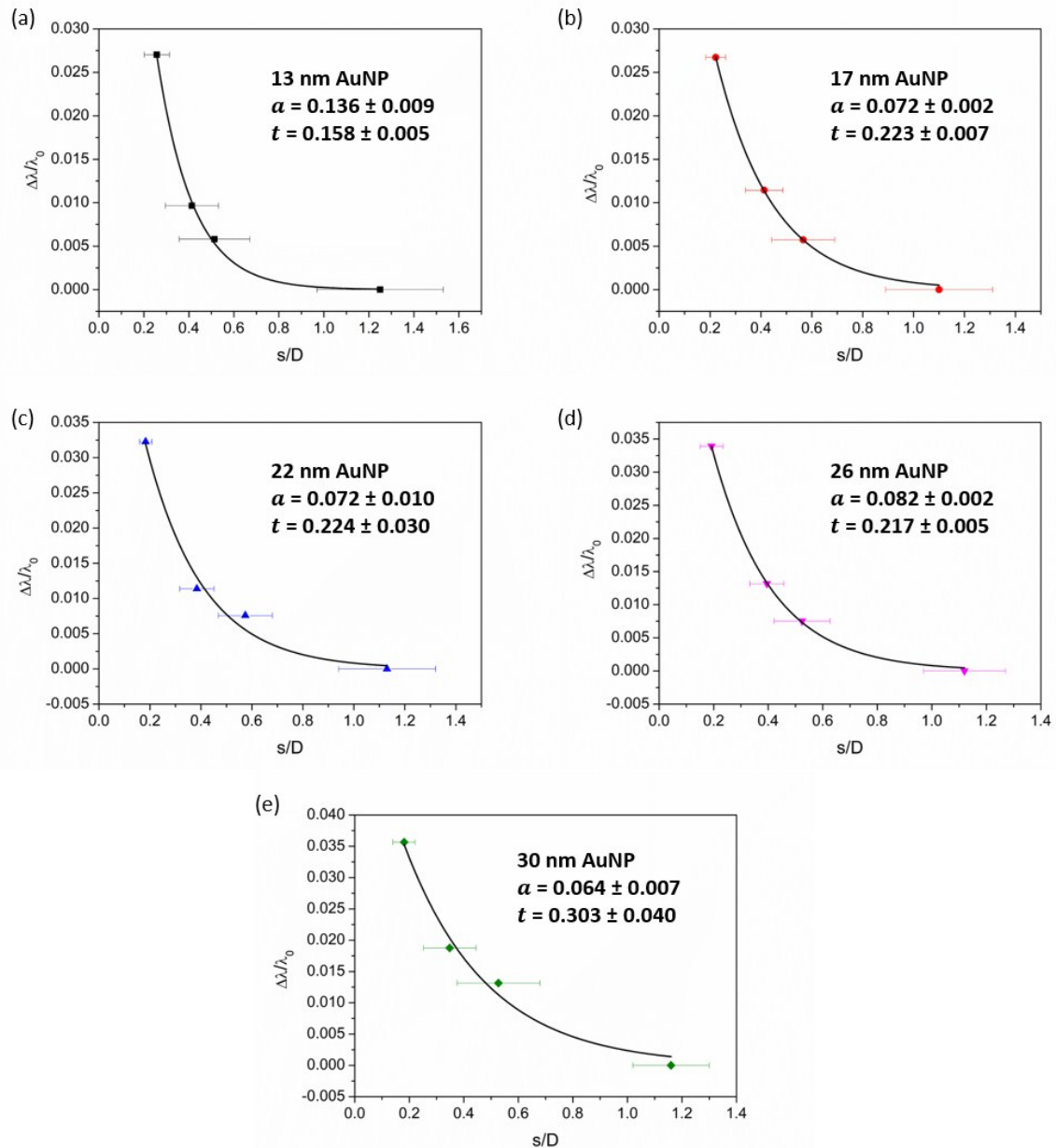


Figure S12. Fractional surface plasmon shift ($\Delta\lambda/\lambda_{0PSLA}$) plotted as a function of relative interparticle distance (s/D) for (a) 13 nm AuNPs, (b) 17 nm AuNPs, (c) 22 nm AuNPs, (d) 26 nm AuNPs and (e) 30 nm AuNPs. Lines drawn through points represent optimised exponential curve fitting using equation (1) in main article, using α and t parameters obtained as given.

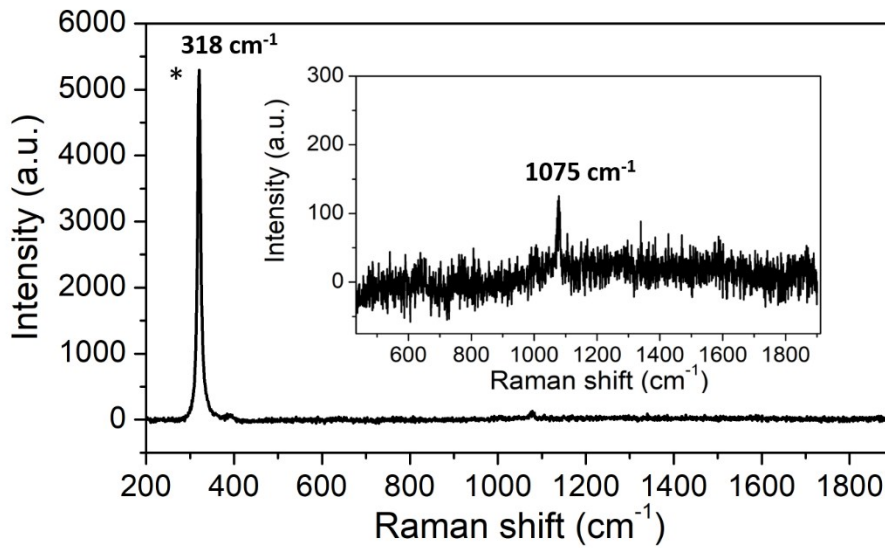


Figure S13. Raman spectrum recorded for a 1 mM 4-MP solution dropped onto a CaF_2 plate. The sample was measured with a 10 s exposure time with a $\lambda_{\text{ex}} = 830 \text{ nm}$ with 1 accumulation and a laser power of 7.6 mW. (*) denotes peak associated with CaF_2 substrate).

Table S7 List of Raman peaks for 30 nm AuNP@200 nm PSLA4 composites exposed to 4-MP.

30 nm AuNP@200 nm PSLA4	Literature Values ^{4#}	Vibrational
Measured Raman Band Position	Raman Band Position	Assignment\$
339 cm^{-1}	331 cm^{-1}	10b
387 cm^{-1}	392 cm^{-1}	7a
633 cm^{-1}	636 cm^{-1}	12
699 cm^{-1}		
820 cm^{-1}	823 cm^{-1}	6a
1002 cm^{-1}	1003 cm^{-1}	18a
1075 cm^{-1}	1075 cm^{-1}	1
1164 cm^{-1}	1169 cm^{-1}	9a
1269 cm^{-1}		13
1485 cm^{-1}	1488 cm^{-1}	19a
1575 cm^{-1}	1583 cm^{-1}	8b
1587 cm^{-1}	1594 cm^{-1}	8a

solution measurements from reference⁴ ($1 \times 10^{-6} \text{ M}$, neutral pH), \$ denoted in Wilson notation

Table S8 Table showing the surface area (SA) available for 4-MP binding per composite, the number of 4-MP molecules per composite and the normalised intensity at 1075 cm⁻¹ for each measured 200 nm composite family.

AuNP Size	Avg AuNPs / Composite	Total AuNP Surface Area	No. 4-MP per Composite	Mol. of 4-MP per Composite	Relative Number *	Measured Int. at 1075 cm ⁻¹ \$	Weighted Int. at 1075 cm ⁻¹ \$
13 nm AuNP (200 nm PS)	159 ± 14 AuNPs	(8.44 ± 0.74) x 10 ⁴ nm ²	(2.56 ± 0.23) x 10 ⁵	(4.25 ± 0.37) x 10 ⁻¹⁹	1.10	351 ± 179 (SD = 50 %)	319 ± 162
17 nm AuNP (200 nm PS)	114 ± 10 AuNPs	(10.26 ± 0.90) x 10 ⁴ nm ²	(3.11 ± 0.27) x 10 ⁵	(5.16 ± 0.45) x 10 ⁻¹⁹	1.34	2473 ± 421 (SD = 17 %)	1819 ± 314
22 nm AuNP (200 nm PS)	77 ± 8 AuNPs	(11.70 ± 1.2) x 10 ⁴ nm ²	(3.55 ± 0.37) x 10 ⁵	(5.89 ± 0.61) x 10 ⁻¹⁹	1.53	13121 ± 1745 (SD = 13 %)	8576 ± 1140
26 nm AuNP (200 nm PS)	38 ± 3 AuNPs	(8.07 ± 0.64) x 10 ⁴ nm ²	(2.45 ± 0.19) x 10 ⁵	(4.06 ± 0.32) x 10 ⁻¹⁹	1.06	30681 ± 4178 (SD = 14 %)	28945 ± 3941
30 nm AuNP (200 nm PS)	26 ± 3 AuNPs	(7.35 ± 0.85) x 10 ⁴ nm ²	(2.23 ± 0.26) x 10 ⁵	(3.70 ± 0.430 x 10 ⁻¹⁹)	1	68914 ± 14322 (SD = 21 %)	68914 ± 14322

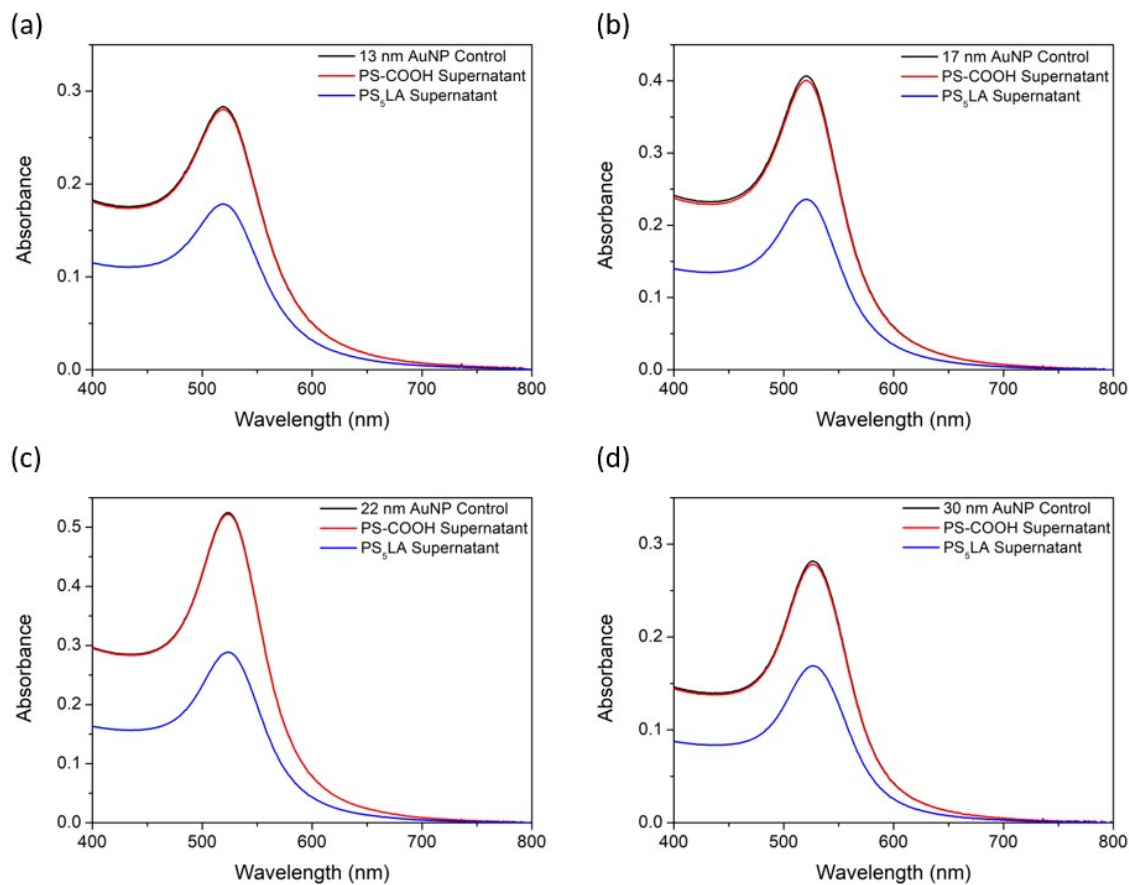


Figure S14. UV-visible spectra of AuNP control and supernatants after incubation with 5.3 μm PS-COOH and PSLA4 for (a) 13 nm AuNPs, (b) 17 nm AuNPs, (c) 22 nm AuNPs and (d) 30 nm AuNPs. All spectra were taken in ddH₂O at ambient temperature and pressure.

Table S9 Summary of loadings, in % PS surface area covered, determined by UV-visible and AAS for the different AuNP families immobilised on the 5.3 μm PSLA4 particles, along with the equivalent loadings for the AuNPs on 200 nm PSLA4 particles.

	13 nm AuNP	17 nm AuNP	22 nm AuNP	30 nm AuNP
UV-Vis Coverage	17.9 %	19.9 %	21.5 %	16.9 %
AAS Coverage	17.4 %	19.1 %	21.7 %	17.3 %
Avg. Coverage	17.7 %	19.5 %	21.6 %	17.1 %
200 nm PSLA4	16.8 %	20.4 %	23.3 %	15.2 %

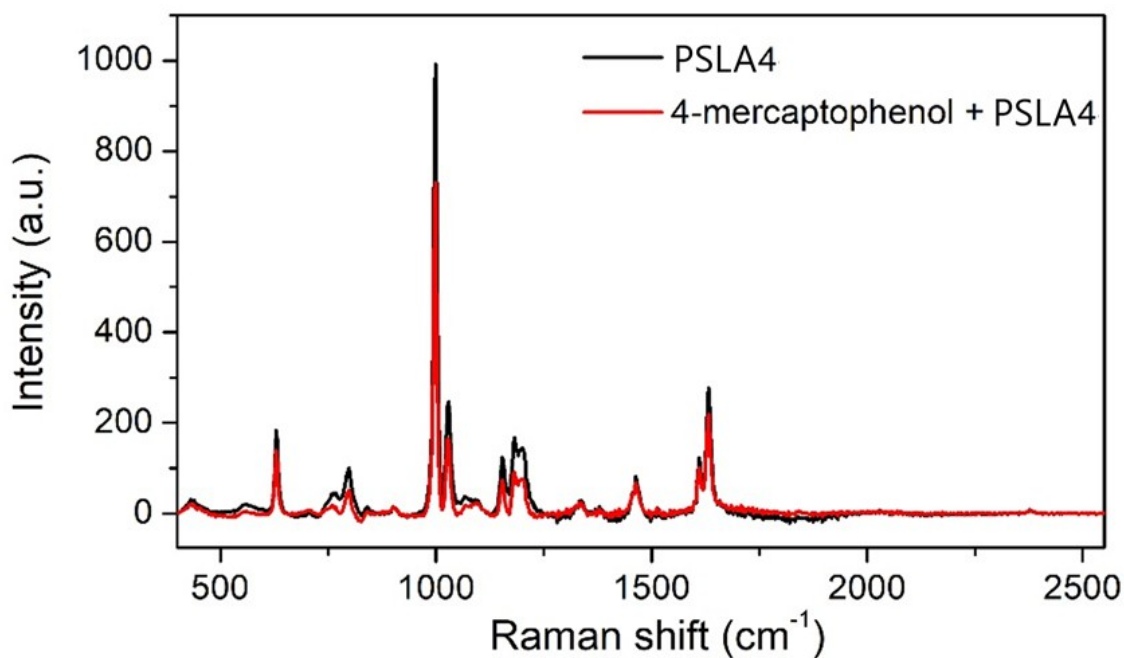


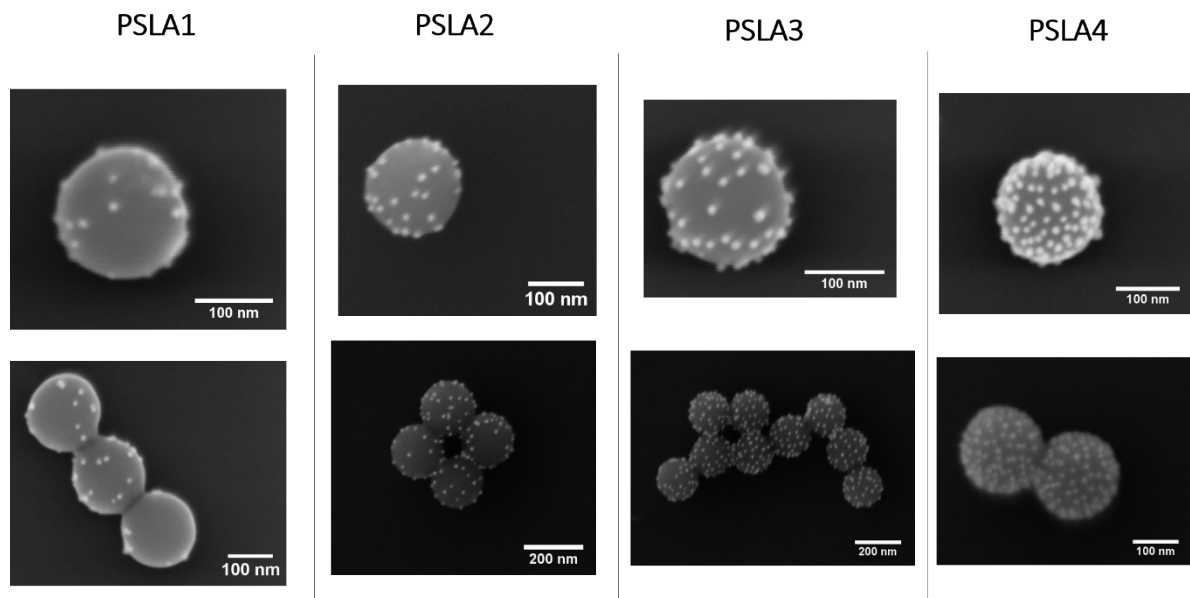
Fig S15. Raman spectra for both PSLA4 particles (black) and PSLA4 incubated with 4-MP (red). Spectra were recorded in ddH₂O using the same laser source ($\lambda_{\text{ex}} = 785 \text{ nm}$) for both trapping and SERS excitation with a laser power of 20 mW at the objective, a 0.2 s exposure time and 1 accumulation.

Table S10 Table showing the surface area (SA) available for 4-MP binding per composite, the number of moles of 4-MP per composite and the intensity (Int.) per mole of 4-MP at 1075 cm⁻¹ for each 5.3 μm PSLA4 family.

AuNP Size	Avg AuNPs / Composite	Total AuNP Surface Area	No. 4-MP per Composite	Mol. of 4-MP per Composite	Relative Number *	Measured Int. at 1075 cm ⁻¹ \$	Weighted Int. at 1075 cm ⁻¹ \$	Int. at 1075 cm ⁻¹ per mole
13 nm AuNP (5.3 μm PS)	117700 ± 15200	$(6.25 \pm 0.81) \times 10^7 \text{ nm}^2$	$(1.89 \pm 0.25) \times 10^8$	$(3.14 \pm 0.41) \times 10^{-16}$	1.03	$156 \pm 27 \text{ (SD = 17 %)}$	151 ± 26	$(4.96 \pm 0.85) \times 10^{17}$
17 nm AuNP (5.3 μm PS)	75800 ± 8600	$(6.88 \pm 0.78) \times 10^7 \text{ nm}^2$	$(2.08 \pm 0.24) \times 10^8$	$(3.46 \pm 0.39) \times 10^{-16}$	1.14	$142 \pm 27 \text{ (SD = 19 %)}$	124 ± 24	$(4.10 \pm 0.78) \times 10^{17}$
22 nm AuNP (5.3 μm PS)	50200 ± 4800	$(7.64 \pm 0.73) \times 10^7 \text{ nm}^2$	$(2.31 \pm 0.22) \times 10^8$	$(3.84 \pm 0.37) \times 10^{-16}$	1.24	$388 \pm 81 \text{ (SD = 21 %)}$	366 ± 76	$(1.01 \pm 0.21) \times 10^{18}$
30 nm AuNP (5.3 μm PS)	21300 ± 2700	$(6.02 \pm 0.76) \times 10^7 \text{ nm}^2$	$(1.82 \pm 0.23) \times 10^8$	$(3.03 \pm 0.38) \times 10^{-16}$	1	$1220 \pm 230 \text{ (SD = 19 %)}$	1220 ± 230	$(4.02 \pm 0.76) \times 10^{18}$

4

13 nm AuNPs



17 nm AuNPs

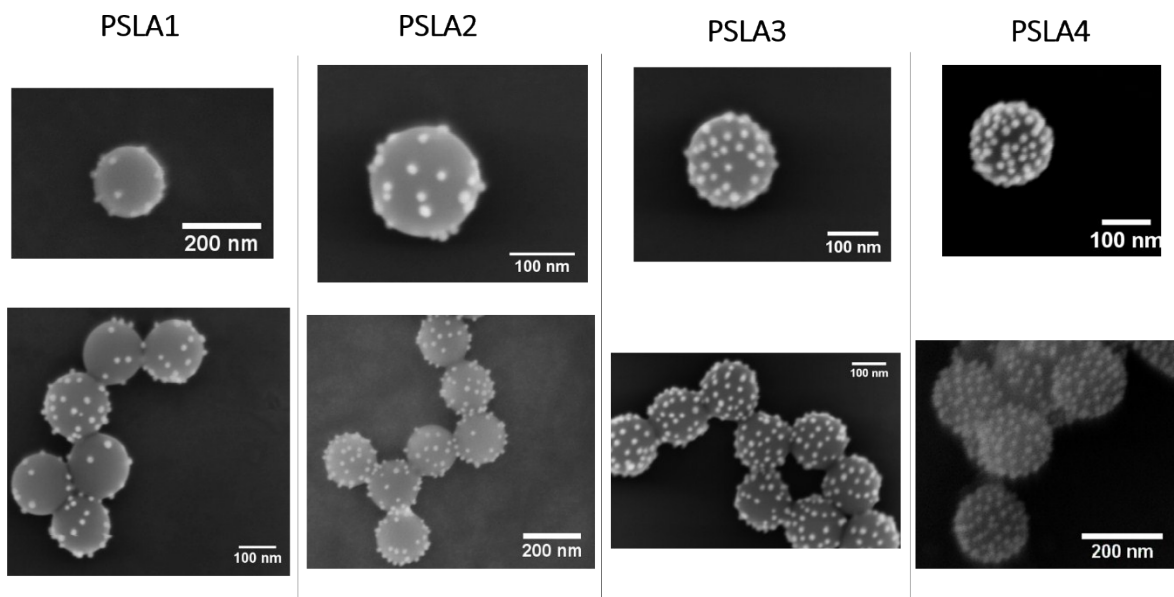


Fig S16. SEM images of 13 nm AuNP@PSLA composite families

Fig S17. SEM images of 17 nm AuNP@PSLA composite families

22 nm AuNPs

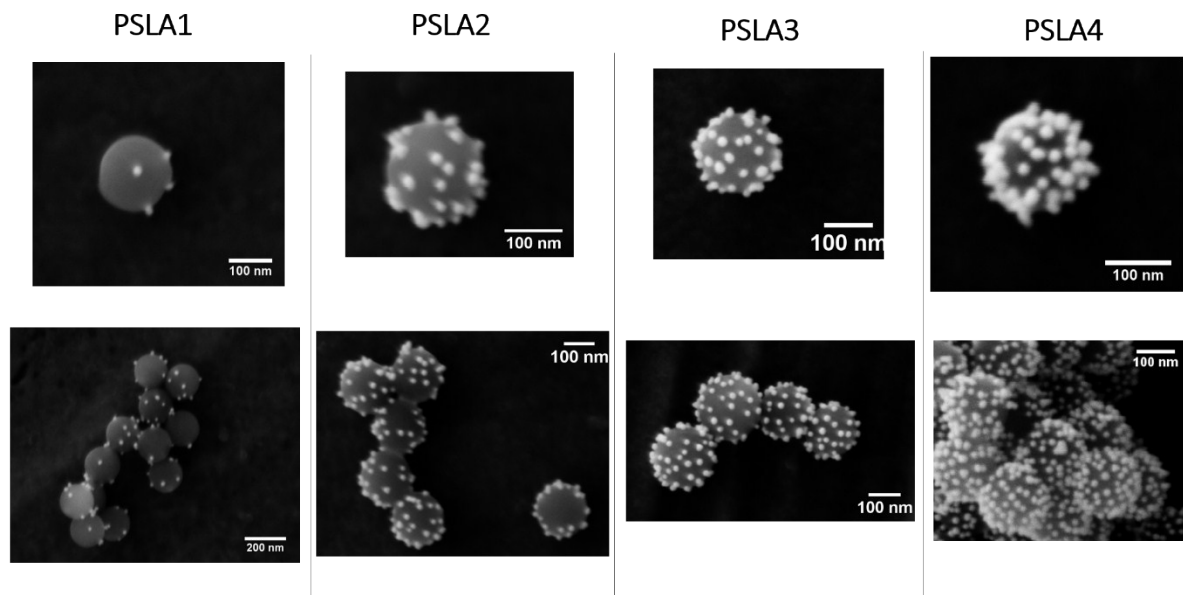


Fig S18. SEM images of 22 nm AuNP@PSLA composite families

26 nm AuNPs

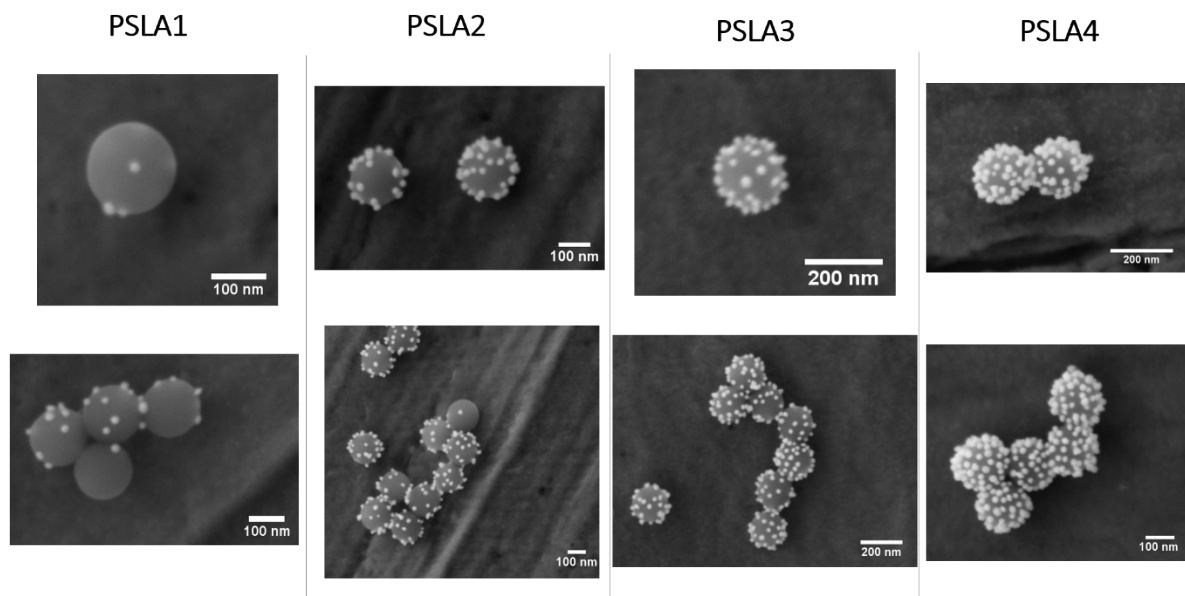


Fig S19. SEM images of 26 nm AuNP@PSLA composite families

30 nm AuNPs

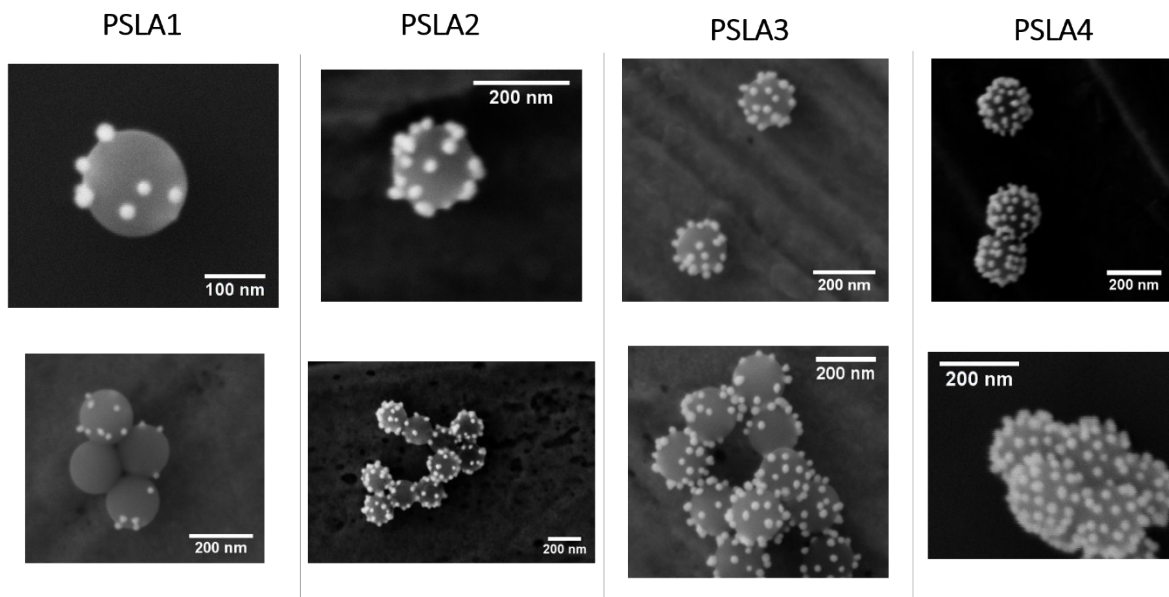


Fig S20. SEM images of 30 nm AuNP@PSLA composite families

References

- 1 H. Y. Song, M. H. Ngai, Z. Y. Song, P. A. MacAry, J. Hobley and M. J. Lear, *Org. Biomol. Chem.*, 2009, **7**, 3400–3406.
- 2 Y. Wang, K. El-boubbou, H. Kouyoumdjian, B. Sun, X. Huang and X. Zeng, *Langmuir*, 2010, **26**, 4119–4125.
- 3 N. G. Bastús, J. Comenge and V. Puntes, *Langmuir*, 2011, **27**, 11098–11105.
- 4 H. M. Lee, M. S. Kim and K. Kim, *Vib. Spectrosc.*, 1994, **6**, 205–214.